Numerical Study of Metal Fatigue in a Superelastic Anchoring Stent Embedded in a Hyperelastic Tube

Milton A. DeHerrera, Ph.D
Edwards Lifesciences LLC
1 Edwards Way
Irvine, CA 92614
USA

Wei Sun, Ph.D
Department of Mechanical Engineering, University of Connecticut
Storrs, CT 06269
USA

Abstract: In this study we compare various way of quantifying high cycle radial fatigue behavior in a percutaneous Mitral repair device using Goodman methods. In order to provide an improved representation of the tissue-device interaction, we use an Ogden hyperelastic model to simulate the native vessel with parameters obtained from pressure-diameter test data of human cadaver heart coronary tissue, and published data presented in previous work. We also examine how the computed peak tensile strains at the surface of this device differ from (a)The values computed at integration points in the 3D and (b) The same integration point values extrapolated to the nodal points and averaged over adjacent elements.

Keywords: Abaqus Explicit, Abaqus Standard, Cardiovascular Therapy, Constitutive Model, Contact, Fatigue, Fatigue Life, Hyperelasticity, Implantable Medical Device, Mass Scaling, Minimally Invasive Surgery, Mitral Valve Repair, NiTinol, Percutaneous Devices, Ogden Model, Percutaneous Stent Delivery, Superelasticity, Tissue Modeling, UMAT, VUMAT

1. Introduction

This paper analyzes the strains in the proximal anchor for a mitral repair device being developed at Edwards Lifesciences. Our aims are to:

1. Provide a quantitative comparison between modeling a device embedded in a rigid enclosure versus one in a hyperelastic deformable enclosure.
2. Compare results from hyperelastic enclosure using data from human cadaver heart coronary tissue and published data for the Great Saphenous Vein (DeHerrera, Sun, 2007).
3. Study the difference in peak strains computed at different topological locations.

The first phase of this study consists of simulating crimping of the stent to a smaller OD with a subsequent cyclic radial load to help evaluate pulsatile fatigue behavior in the stent. The second phase analyzes the behavior of the stent when deployed in a hyperelastic tube that mimics the Coronary Sinus (CS) undergoing a cycled pressure loading. The final phase compares the peak

tensile strains obtained from (1) integration points at the interior of the C3D8R elements, (2) averaged values at the nodal points extrapolated from the aforementioned integration points and (3) the one integration point in each membrane surface element coating the free surface of the C3D8R elements.

2. Overview of initial FEA model

The proximal anchor can be thought of as an elastic lattice, deriving its strength from the joints and bending action of component struts. Because of the lack of symmetry in this part, the entire anchor has been modeled. When the final solid mesh was generated, its free surface was coated by very thin membrane elements to better capture the true state of strain at the device's surface.

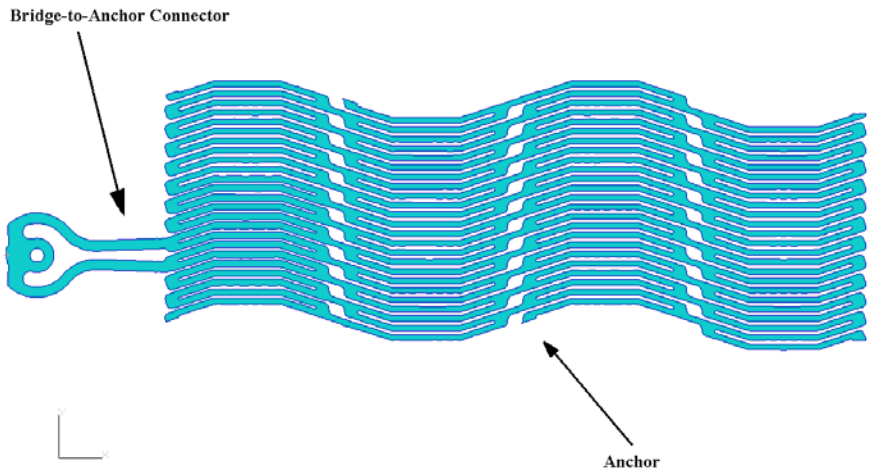

Figure 1. Original flat CAD geometry used to define proximal anchor.

3. Analysis model

The analysis was run with Abaqus/Explicit release 6.8-2 on a 12-CPU Linux cluster running SuSE 9.0. We used C3D8R hexahedral elements for deformable domains representing the actual device, and M3D4R membrane elements for the rigid domains and for the surface elements coating the 3D elements. The main body of the undeformed anchor model is approximately 21mm long, and 26mm long if we include the bridge-to-anchor connector. The wall clock run times of the three models were as follow:

Rigid sleeve model	14h:28m:05s
Hyperelastic tube model 1 (Great Saphenous Vein data)	42h:23m:50s
Hyperelastic tube model 2 (Human cadaver data)	41h:49m:01s.

The topological FEA description of the model is as follows:

Element Sets	#/type of elements	# of nodes
Anchor	114220/C3D8R	163596
Coronary Sinus (CS)	43200/C3D8R	52272
Coating membrane	90288/M3D4R	90212
"Rigid" sleeve	2232/M3D4R	2268

We have used the Abaqus Superelastic model for the anchor, a hyperelastic Ogden model for the coronary sinus (CS) and isotropic elasticity for the coating elements. The Abaqus Superelastic model is based on the work of (Auricchio, et al 1997), (Lubliner, et al 1996), with extensions by (Rebelo, 2002). A more detailed discussion is given in (DeHerrera, et al, 2004). Parameters for the superelastic material model were obtained from dogbone samples tested at Edwards Lifesciences. Data for the Ogden model was generated by curve-fitting data (Stooker, et al 2003), and enhanced by pressure-diameter data from human cadaver coronary veins (Krams, 2004). Figure 2 illustrates the undeformed 3D solid mesh used in this study.

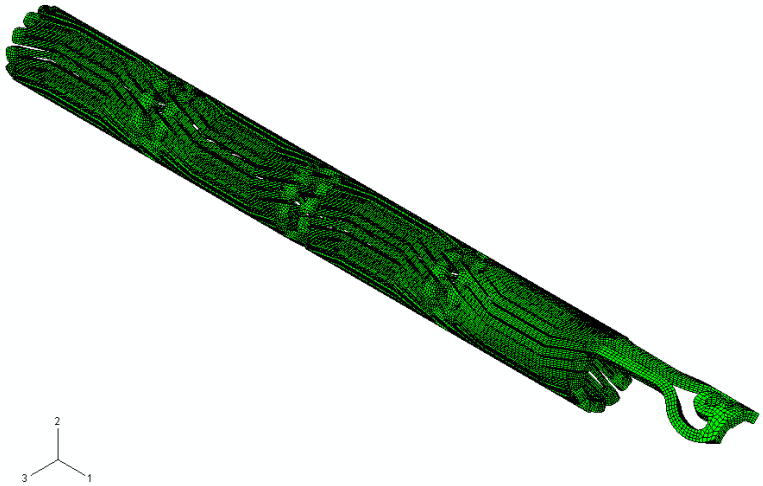

Figure 2. Undeformed mesh of proximal anchor model.

4. Hyperelastic model of the Coronary Sinus

There is a dearth of experimental data on the physical environment in the coronary sinus, and even less on its mechanical properties. The closest applicable *published* human data we found was from

(Stooker, et al, 2003) describing the pressure-diameter relationship in the Greater Saphenous Vein. An internal study at Edwards Lifesciences (Krams, 2004) on cadaver coronary tissue provided a separate and more realistic set of data. We have chosen both of these sets of data, in combination with the Ogden constitutive model to mechanically represent the coronary sinus. A typical Ogden model is of the form:

$$W = \sum_{i=1}^{N} \frac{2\mu_i}{a_i^2}(\lambda_1^{a_i} + \lambda_2^{a_i} + \lambda_3^{a_i} - 3) \qquad (1)$$

where W is the strain energy density, μ_i and a_i are material constants and λ_i are the principal stretches. Because we are using Abaqus/Explicit, a slight amount of compressibility equivalent to a $\nu = 0.499$ was enabled in the Ogden formulation. A separate quarter-tube model for the vein was used to generate the Ogden material parameters for both sets of data.

5. Using membrane elements to better capture surface strains

There has always been some concern with finite element analyses using solid elements that the most exact characterization of field quantities occurs at the integration points, which are located in the interior of the part being modeled, whereas often (particularly where significant bending or torsion is involved) the largest strains occur at the surface, which are traditionally available only by extrapolation from the integration points to the nodal points using the element's shape functions. The *raison d'etre* for using M3D4R membrane elements in this study is to "trick" the solver into providing surface values that are more exact and are not interpolated, and to see how much they differ from extrapolated nodal values and integration point values in the solid elements. Since we are only concerned with strains, we use a simple isotropic elastic material model for the coating membrane with a modulus $E << E_A$, where E_A is the initial austenitic modulus of the device. The membrane element's thickness is set to $1/1000^{th}$ the electropolished tube thickness.

6. Simulation of anchor crimping by a rigid surface

In a previous paper (DeHerrera, Sun, 2007) we described how the model is crimped with a rigid surface to a target diameter and then cycled (via pressure or with the same rigid surface) to mimic a fatigue cycle. We again should note that, even though we speak of a "rigid" surface, it is mechanically described by an elastic material law, albeit with an Elastic modulus $>> E_A$.

7. Mechanical fatigue analysis methodology: Goodman Plot/Diagram

When the mitral repair device is implanted in the coronary sinus, it will be subjected to a pulsatile load that will fatigue the device. Quantitative studies of material fatigue often make use of a Goodman-Haigh plot/diagram, where the abscissa represents the mean stress or strain at a point and the ordinate represents the amplitude of stress or strain at the same point. The distinction between a "Goodman plot" and a "Goodman diagram" is that the former is a plot of (mean,amplitude) stress or strain ordered pairs, and the latter also includes a Constant Life Curve, which plots the boundary beyond which fatigue failure is expected to occur. Because of the proprietary nature of the experimentally developed Constant Life curves, we will only present Goodman plots. In the first phase of this study, where the anchor displacement is being driven by a

cylindrical rigid surface that can only impart motions in the radial direction, the displacement field can be adequately tracked by a mean rigid surface diameter and the displacement amplitude about that mean diameter. It is convenient, but by no means necessary, to use a sinusoidal function to describe the displacement amplitude variation about some mean diameter value. By studying changes in maximum tensile strain that occur in the anchor during such a cycle, fatigue effects can be evaluated via a Goodman plot/diagram.

Given a rigid surface with mean diameter D and displacement amplitude A, we use the notation "fat" or "thin" to denote the configurations $D_{fat} = D + A$ and $D_{thin} = D - A$, respectively. The mean peak tensile strain in the anchor at a given node is calculated from the equation:

$$\varepsilon_{meanD} = \tfrac{1}{2} |\varepsilon_{fat} + \varepsilon_{thin}| \qquad (2)$$

where ε_{fat} and ε_{thin} are the peak tensile strains at said node in the D_{fat} and D_{thin} configurations, respectively. Similarly, the amplitude $\Delta\varepsilon$ is given by:

$$\Delta\varepsilon = \tfrac{1}{2} |\varepsilon_{fat} - \varepsilon_{thin}| \qquad (3)$$

It is unfortunate fact that many have chosen to call $\Delta\varepsilon$ the "half-amplitude" what everyone else (based on the study of time series and Fourier analysis) refers to as "amplitude." We shall refer to $\Delta\varepsilon$ as "amplitude" from hereon forth.

Strictly speaking, the above equations for ε_{meanD} and $\Delta\varepsilon$ are approximations. The reason is, unlike an uniaxial state of stress/strain, the principal directions of ε_{fat} and ε_{thin} are not always coincident. However, a study conducted by the first author (DeHerrera, 2006) concluded that for an applied radial displacement on this type of stent-like structure at these strain levels, the error is small.

Since we are mainly concerned with peak tensile strains, field variables SDV24 and LEP3 were used for the solid elements the coating membrane elements, respectively. Both field variables give the same result when there are no annealing steps. There are several ways of obtaining the necessary data to generate the Goodman points (ε_{meanD} , $\Delta\varepsilon$). One is to extract SDV24/LEP3 at "fat" and "thin" configurations using the Abaqus/Viewer **Report/Field Output/Integration Point** or **Report/Field Output/Unique Nodal** feature, and another is to Create Output from Fields, the latter being particularly useful to display contour plots of mean and amplitude peak strains. In the former case, output files for each configuration were processed through a FORTRAN program that formed and sorted the Goodman points, scaled them to a percentage, and the data was imported back into Abaqus/Viewer as XY-data. Goodman plots are sometimes difficult to interpret when there are thousands of points, and so we plot a Goodman "Skyline" plot where all the Goodman points are placed in 200 bins of width **B**, where

$$\mathbf{B} = [\max(\varepsilon_{meanD})]/200 \qquad (4)$$

To ensure consistency in the skyline plots, all Skyline plots in this study were made assuming $\max(\varepsilon_{meanD}) = 3.2$ %

8. Displacement-controlled ("rigid" tube) fatigue study

The applied boundary conditions used in the displacement-controlled rigid tube analysis represent the best estimates that were available at the start of this project, and before actual devices were implanted in animal or human trials. In retrospect, these were quite conservative, but serve to illustrate the continuing improvement in our analyses as the uncertainty in boundary conditions is reduced. The initial baseline geometry for crimping was obtained from a forming analysis described in (DeHerrera, Sun, 2007) with slightly different material properties. After crimping the anchor to an OD = 13.5mm, a sinusoidal radial displacement $\Delta R = \pm 0.25$mm was applied through the rigid surface to simulate a cyclic load, allowing the extraction of the Goodman points (ε_{meanD}, $\Delta\varepsilon$). Figure A-1 in Appendix A illustrates the proximal anchor in surrounded by a translucent rigid surface. Figures 3 and 4 show the corresponding Goodman and Skyline plots for an anchor crimped to OD = 13.5mm with the aforementioned cyclic radial displacement and with Goodman points computed at (1) integration points of C3D8R elements (2) element nodes, extrapolated from the integration points of the C3D8R's and (3) the integration points of the coating membrane elements.

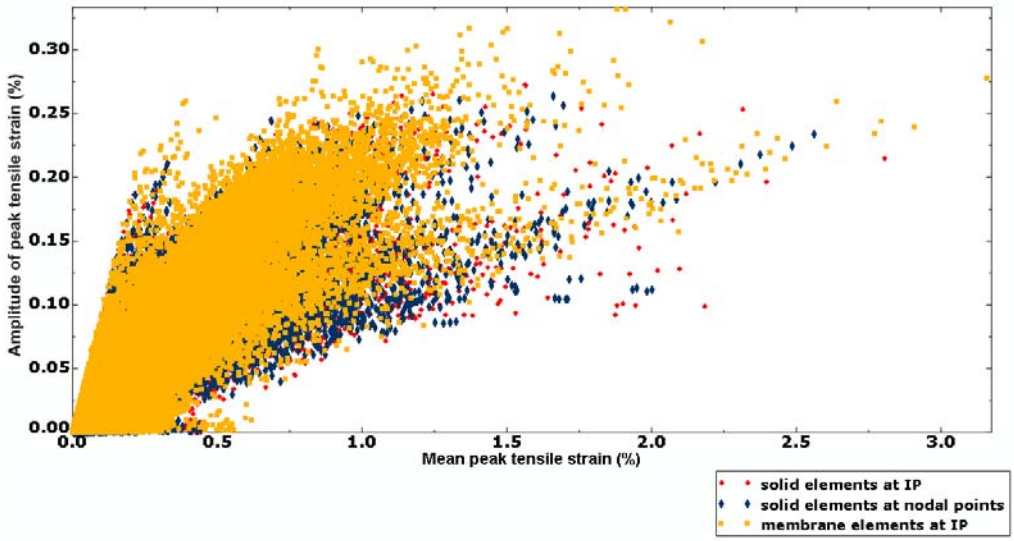

Figure 3. Displacement-controlled Goodman plot for a proximal anchor crimped to OD = 13.5mm with an added axial load to Bridge-to-Anchor Connector, and cycled through $\Delta R = \pm 0.25$mm.

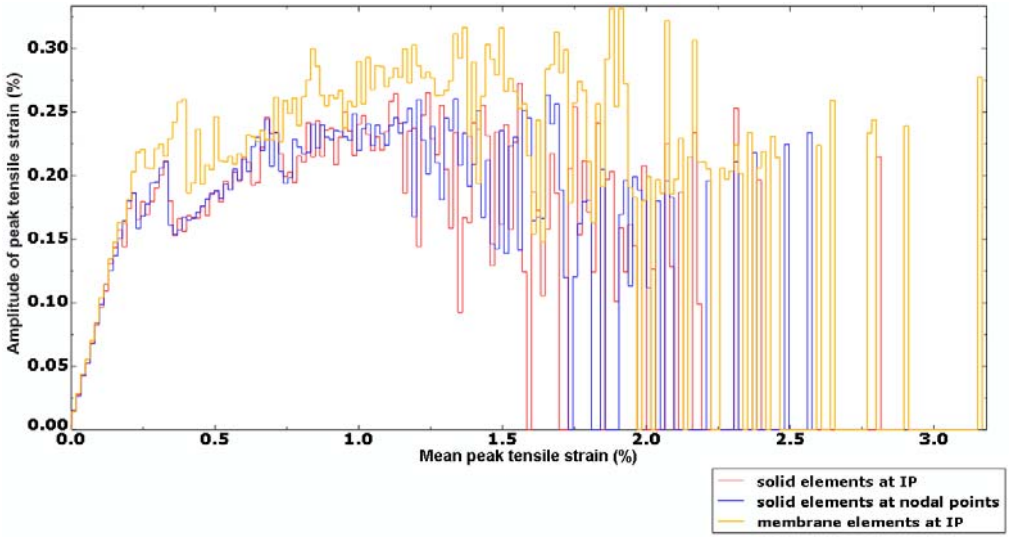

Figure 4. Displacement-controlled Goodman skyline plot for a proximal anchor crimped to OD = 13.5mm with an added axial load to bridge-to-anchor Connector, and cycled through ΔR = ± 0.25mm.

9. Load-controlled fatigue study

A major objective of this study was to see how the anchoring stent deforms in a hyperelastic tube, to see how it compares with the results from a rigid tube. In particular, we want to compare the Goodman plots from a "deformable" load-controlled analysis with those from a "rigid" displacement-controlled analysis. With respect to load boundary conditions in the Coronary Sinus, we initially used a maximum pressure of 5mm Hg based on the work of (Ganong, 1971), but since updated it to 10mm Hg based on (Thubrikar, 2007). For the minimum pressure, we used 0mm Hg.

The initial baseline anchor geometry for crimping was the same used in section 8, with the addition of a hyperelastic tube to model the CS. Two material configurations were and are tagged by the principal investigators' name: Stooker (Stooker, et al, 2003) and Krams (Krams, 2004). The analysis sequence was made up of the following steps:

1. Crimp anchor to an OD of 12mm, which is the ID of the hyperelastic tube representing the coronary sinus.
2. Release the anchor into contacting the CS model.
3. Apply an axial load to account for the expanded device Bridge/spring load.
4. Apply an internal pressure to the CS model, starting a 0mm Hg, ramped up to 10mm Hg

Figure A-2 in Appendix A shows the proximal anchor embedded in a translucent hyperelastic tube representing the CS.

Extraction of the Goodman points (ε_{meanD} , $\Delta\varepsilon$) follows a procedure similar to that used for the displacement-controlled study in section 8. Figures 5 through 8 show the corresponding Goodman and Goodman skyline plots for both Stooker and Krams material configurations. Figure 9 compares skyline plots for the traditional displacement-controlled rigid surface case and the load-controlled Krams case. It can be seen that the Goodman points generated from a load-controlled analysis have a much lower strain amplitude, which implies that imparting a radial motion to the anchor by compression/expansion of a rigid surface with $\Delta R = \pm 0.25$mm was conservative.

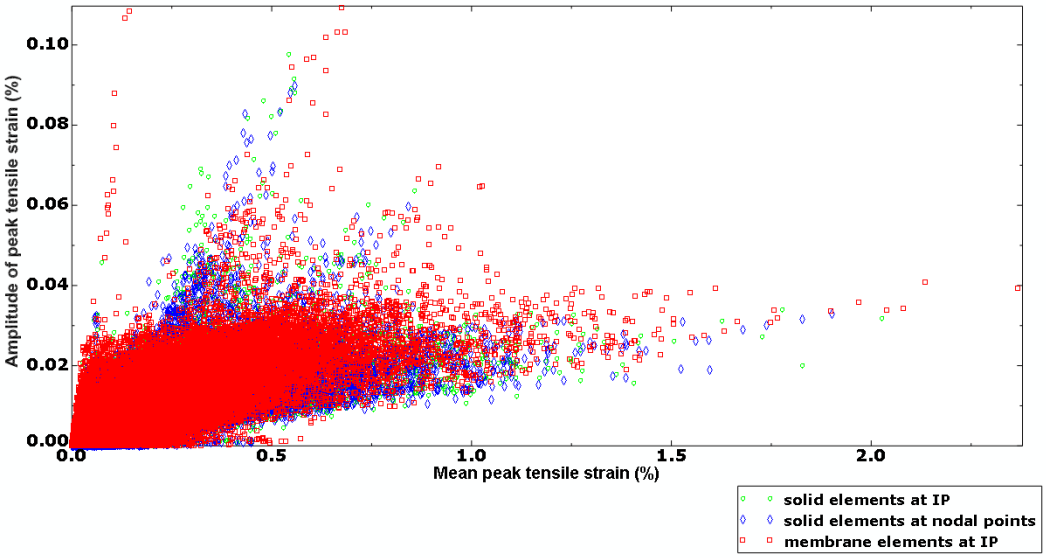

Figure 5. Load-controlled Goodman plots for a proximal anchor embedded in a hyperelastic tube modeled with Stooker material parameters.

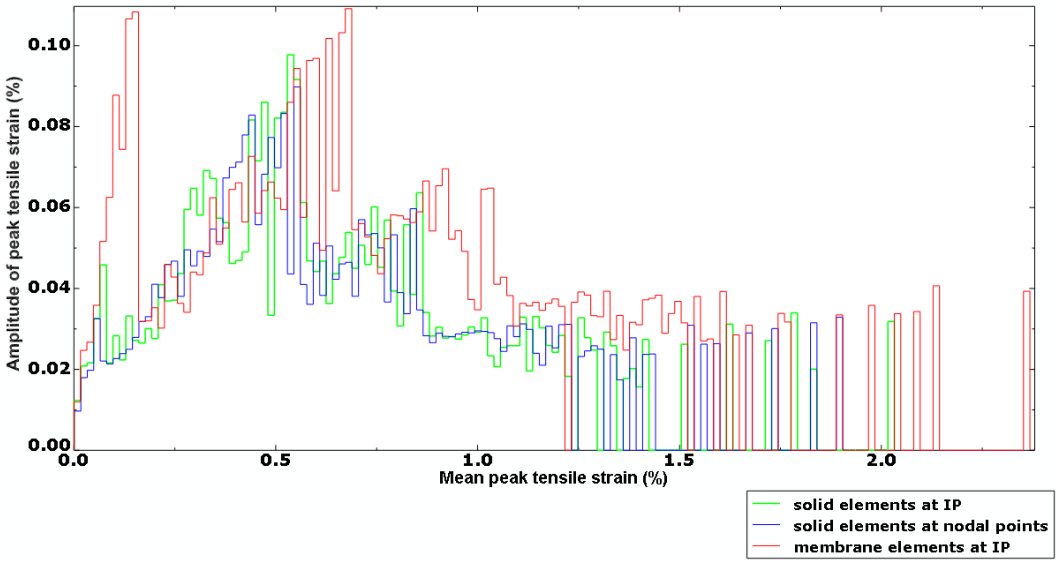

Figure 6. Load-controlled Goodman skyline plots for a proximal anchor embedded in a hyperelastic tube modeled with Stooker material parameters.

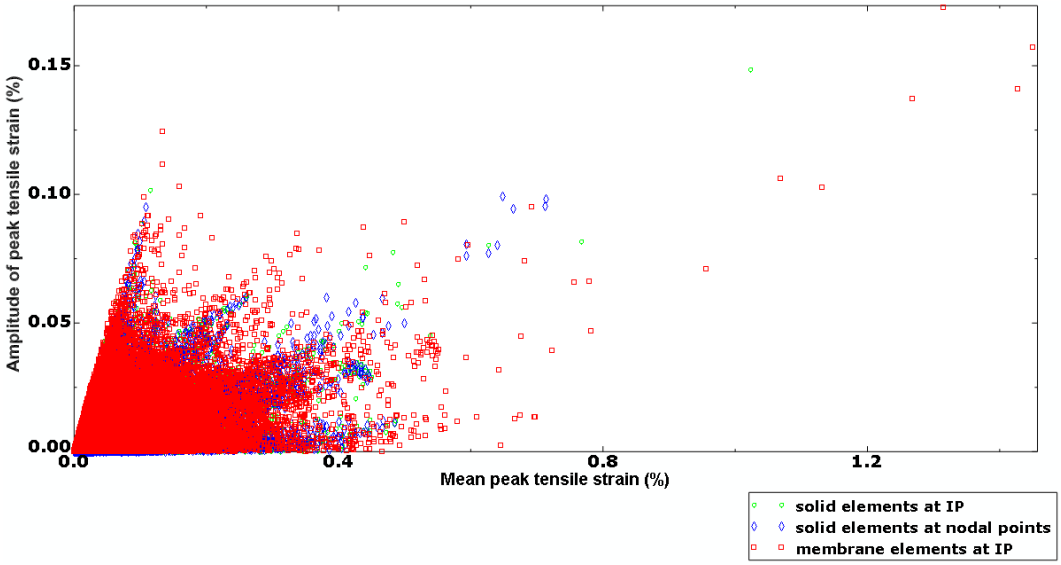

Figure 7. Load-controlled Goodman plots for a proximal anchor embedded in a hyperelastic tube modeled with Krams material parameters.

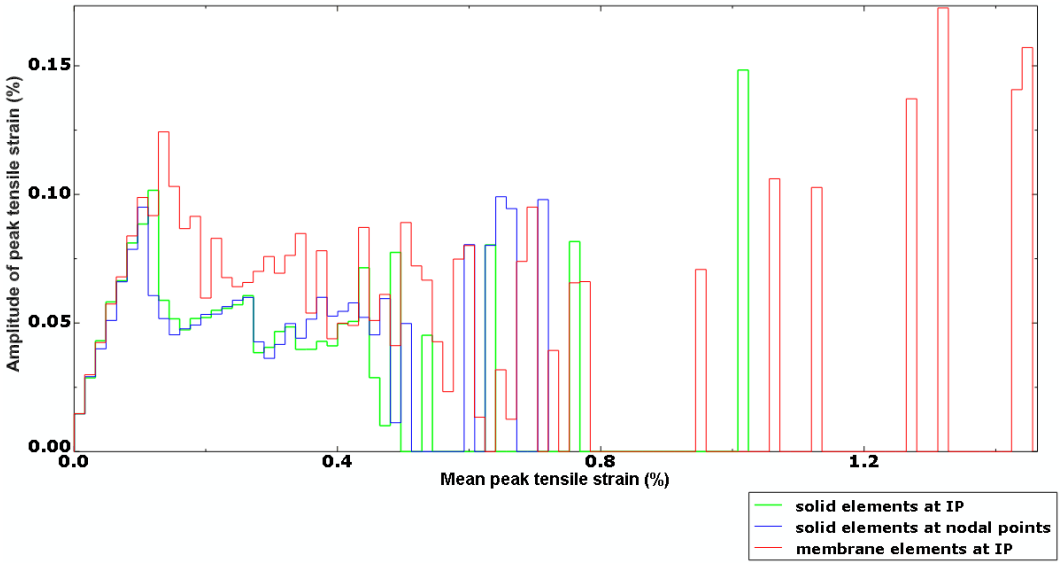

Figure 8. Load-controlled Goodman skyline plots for a proximal anchor embedded in a hyperelastic tube modeled with Krams material parameters.

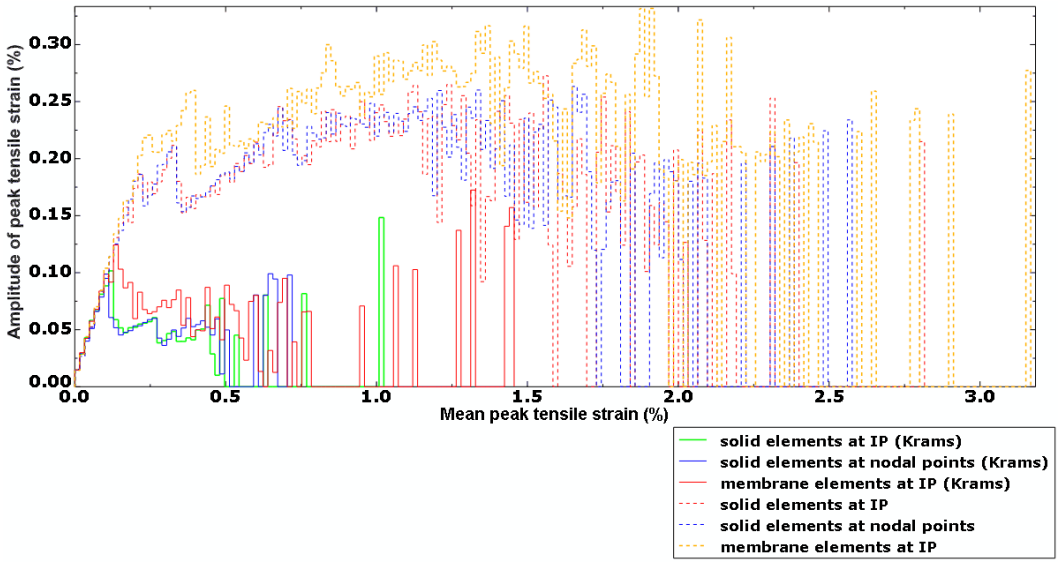

Figure 9. Comparison of Goodman skyline plots from displacement-controlled and Krams load-controlled cases.

10. Contour plots for mean and amplitude of peak tensile strain for proximal anchor embedded in a CS modeled with Krams material parameters

We can easily create contour plots from field data using Abaqus/Viewer. We wish to compare results for mean peak strain and amplitude of peak strain computed at the integration points of the C3D8R's versus those of the M3D4R's. For the sake of brevity, we only compare for the case of a proximal anchor in a CS modeled with Krams material parameters. Using the flexibility provided by Viewer, we display these values in (%) instead of a decimal fraction. Figures 10-11 illustrate the calculated mean and amplitude of peak tensile strains for c3d8r solid elements, and Figures 12-13 illustrate the same for the coating membrane elements. Note that the highest mean and amplitude values occur at nearly the same location for both the solid element mesh and the coating membrane elements.

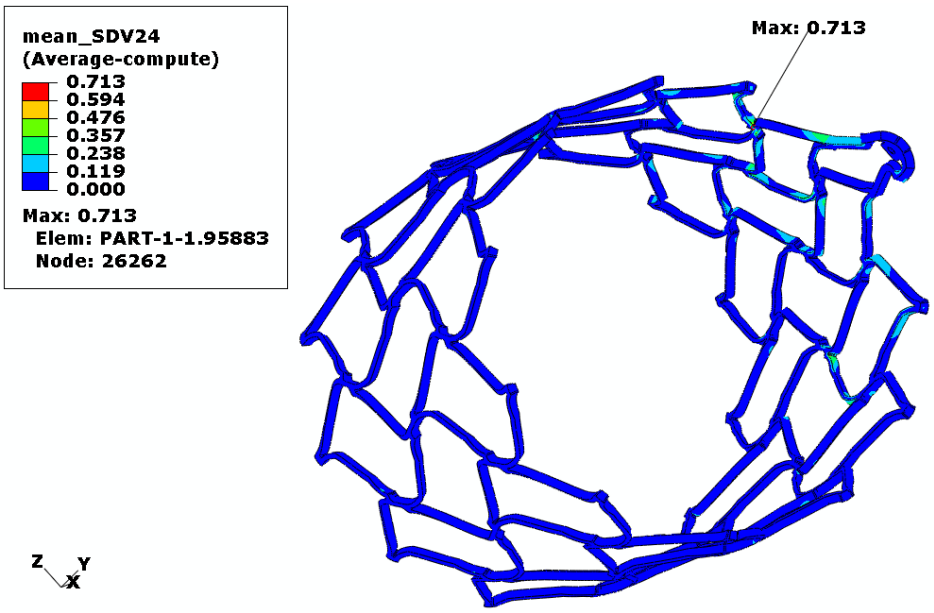

Figure 10. Mean peak tensile strain (%) in solid elements due to pressure cycling from 0mm Hg to 10mm Hg (Anchor embedded in CS with Krams parameters).

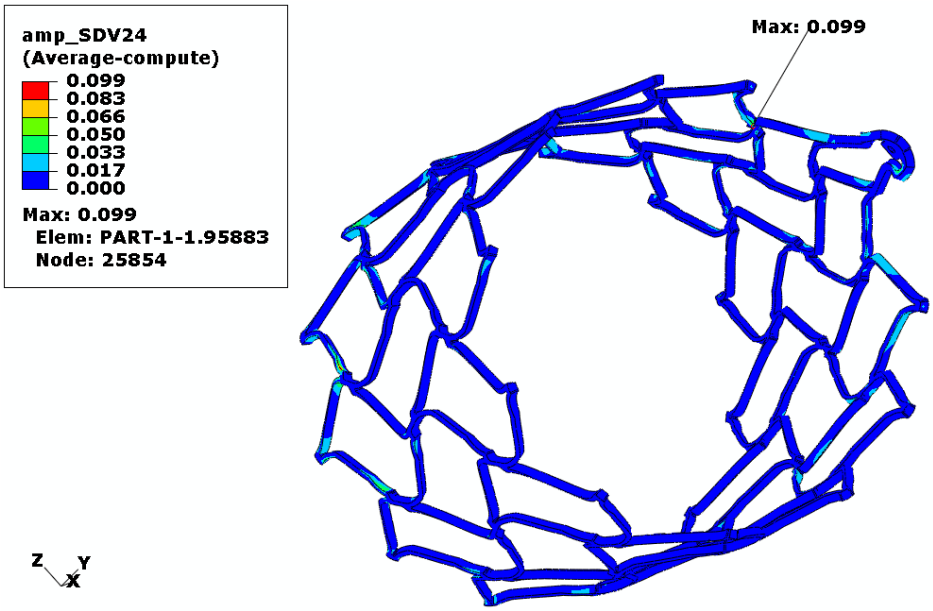

Figure 11. Amplitude of peak tensile strain (%) in solid elements due to pressure cycling from 0mm Hg to 10mm Hg (Anchor embedded in CS with Krams parameters).

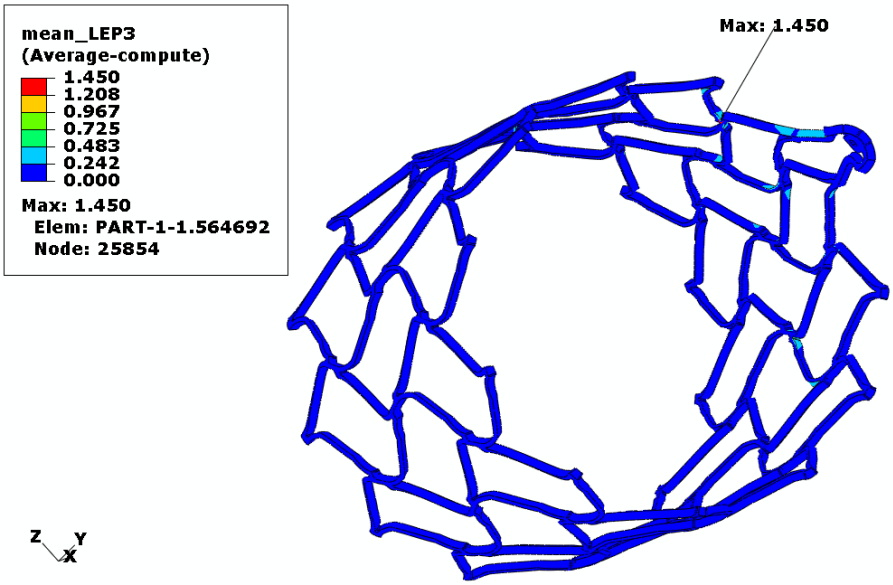

Figure 12. Mean peak tensile strain (%) in membrane coating elements due to pressure cycling from 0mm Hg to 10mm Hg (Anchor embedded in CS with Krams parameters).

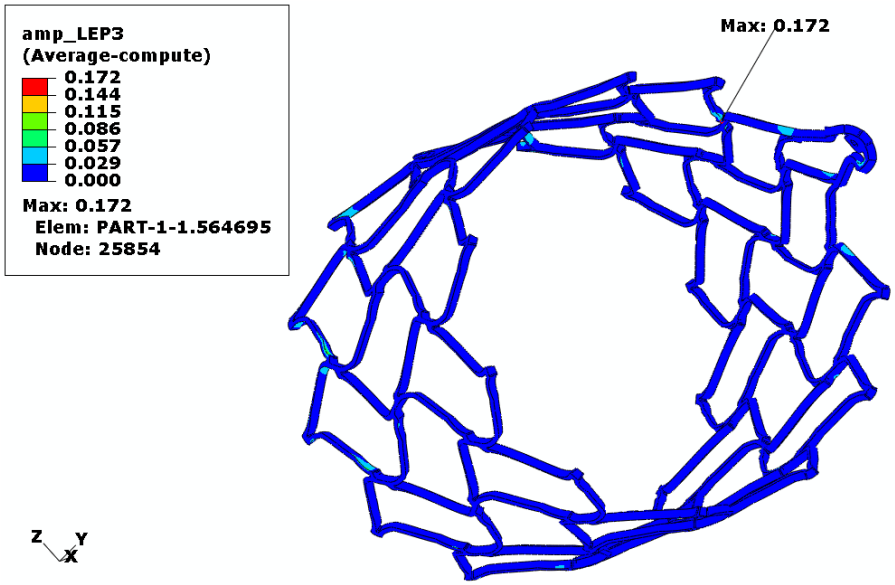

Figure 13. Amplitude of peak tensile strain (%) in membrane coating elements due to pressure cycling from 0mm Hg to 10mm Hg (Anchor embedded in CS with Krams parameters).

11. Discussion and conclusions

A major objective of this study was to compare and evaluate the difference between modeling the proximal anchor of a mitral repair device in a rigid enclosure versus a deformable, hyperelastic enclosure, and to compare the strain values reported at the solid element integration points, results extrapolated to the c3d8r's nodal point and results at the integration point of the membrane coating elements. We have used a right circular cylinder to model the CS, a simplifying geometric representation of the actual conical geometry of the Sinus.

By examining the resulting Goodman plots for each case we conclude that, for the specified boundary conditions in this study:

1. A rigid surface driven proximal anchor model based on initial estimates of radial motion yields conservative results compared to an anchor model embedded (under load boundary conditions) in a hyperelastic tube with properties obtained from human cadaver data, the former giving strain amplitudes that are significantly higher.
2. The mean and amplitudes of peak tensile strains will generally be higher in the coating membrane elements than in solid elements, regardless of whether the latter are reported at integration points or extrapolated to its nodal points.
3. From a Goodman plot perspective, there is little difference between integration point data and extrapolated nodal data in solid elements.

12. References

1. DeHerrera, M. A. and W. Sun "Simulation of the Forming of a Superelastic Anchoring Stent and its Deployment in the Coronary Vein." *Proceedings of the ABAQUS Users' Conference, Paris, France, May 2007, pp. 209 - 223.*

2. Stooker, W, M. Gök, P. Sipkema, H. Niessen, A. Baidoshvili, N. Westerhof, E. Jansen, C. Wildevuur an L. Eijsman "Pressure-Diameter Relationship in the Human Greater Saphenous Vein." *Annals of Thoracic Surgery* **76** (2003), pp. 1533-1538

3. Krams, W. "Delayed Release Implant Radial Durability Test: Final Report, Appendix A." *Edwards Lifesciences LLC* (2004), pp. 20-30 (Proprietary and confidential)

4. Auricchio, F. and R.L. Taylor "Shape-Memory Alloys: Modeling and Numerical Simulations of the Finite-Strain Superelastic Behavior." *Computational Methods in Applied Mechanics and Engineering* **143** (1997), 175-194

5. Auricchio, F., R.L. Taylor and J. Lubliner "Shape-Memory Alloys: Macromodelling and Numerical Simulations of the Superelastic Behavior." *Computational Methods in Applied Mechanics and Engineering* **146** (1997), 281-312

6. Rebelo, N. *Private Communication,* (2002)

7. DeHerrera, M. A. and N. Dang "Finite Element Analysis of a Percutaneous Stent-Mounted Heart Valve." *Proceedings of the ABAQUS Users' Conference, Boston, Massachusetts, June 2004, pp. 209 - 223.*

8. DeHerrera, M.A. "Computation of Mean Peak Strain and Peak Strain Amplitudes due to Cyclic Loading via Exact (Tensor) and Approximate (Scalar) Means." *Edwards Lifesciences Internal Memo(2006)* (Proprietary and confidential)

9. Ganong, William F. **Review of Medical Physiology**. Lange Medical Publications, 1971, pp 426-427.

10. Lubliner, J. and F. Auricchio "Generalized Plasticity and Shape-Memory Alloys." *International Journal of Solids and Structures* **33** (1996), 991-1003

11. Sun, W., M. Scott and M.S. Sacks, "Finite Element Implementation of a Fung Elastic Model for Planar Anisotropic Biological Materials," *Biomechanics and Modeling in Mechanobiology*, November 2005(2-3), pp. 190-199.

12. Thubrikar, M. **Vascular Mechanics and Pathology.** 1st edition, Springer, 2007, pp. 283-285

13. Appendix A

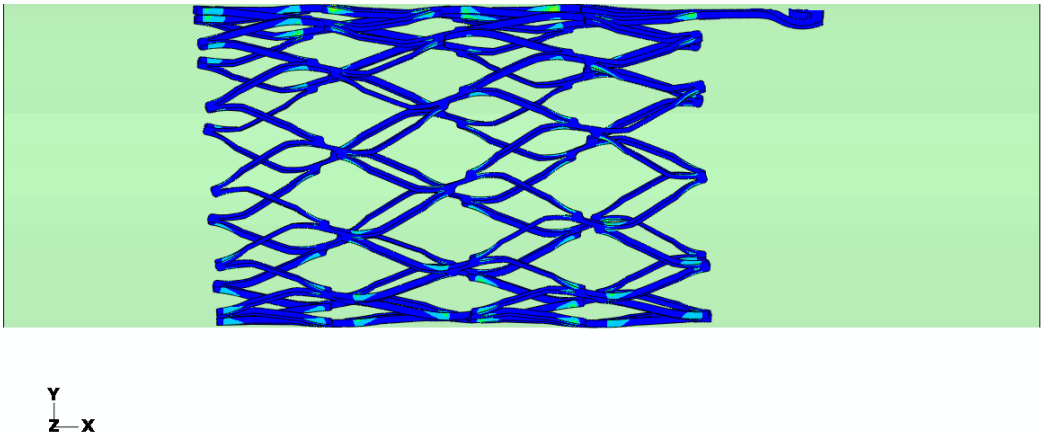

Figure A-1. Deformed configuration of a proximal anchor embedded in a rigid tube at maximum radial compression.

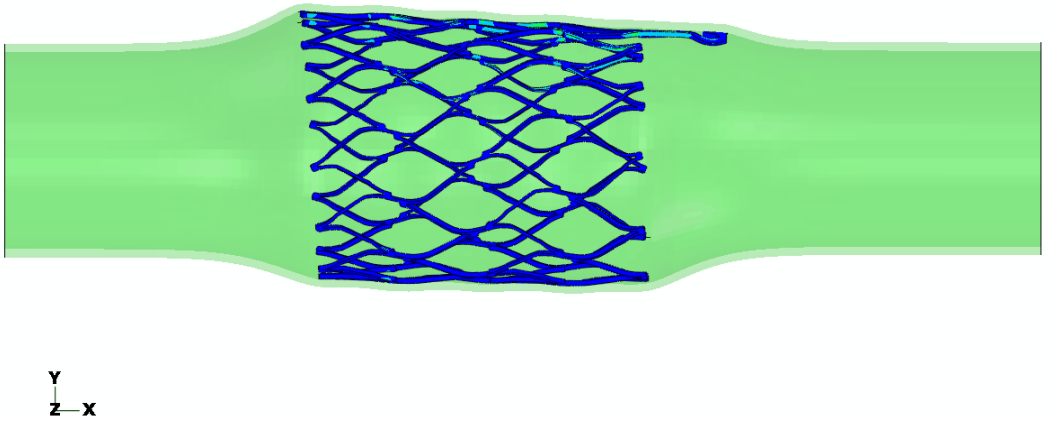

Figure A-2. Deformed configuration of a proximal anchor embedded in a hyperelastic tube with Krams material parameters at 10mm Hg internal pressure.

14. Acknowledgments

Drafts of this paper were reviewed by several technical staff members at Edwards Lifesciences, and by my colleague and former co-worker Mr. Mike LeDuc of Freudenberg-NOK General Partnership.